Available online at www.sciencedirect.com
SCIENCE DIRECT®
Journal of Magnetic Resonance 177 (2005) 212–220
JMR Journal of Magnetic Resonance
www.elsevier.com/locate/jmr

Inert fluorinated gas T_1 calculator

Dean O. Kuethe [a,*], Tanja Pietraß [b], Volker C. Behr [c]

[a] New Mexico Resonance, Albuquerque, NM, USA
[b] Department of Chemistry, New Mexico Institute of Mining and Technology, Socorro, NM, USA
[c] Experimentelle Physik V, Universität Würzburg, Wurzburg, Germany

Received 20 December 2004; revised 25 June 2005
Available online 6 September 2005

Abstract

The physics of spin–rotation interaction in roughly spherical perfluorinated gas molecules has been studied extensively. But, it is difficult to calculate a spin–lattice relaxation time constant T_1 for any given temperature and pressure using the published literature. We give a unified parameterization that makes use of the Clausius equation of state, Lennard-Jones collision dynamics, and a formulaic temperature dependence for collision cross section for rotational change. The model fits T_1s for SF_6, CF_4, C_2F_6, and c-C_4F_8 for temperatures from 180 to 360 K and pressures from 2 to 210 kPa and in mixtures with other common gases to within our limits of measurement. It also fits previous data tabulated according to known number densities. Given a pressure, temperature, and mixture composition, one can now calculate T_1s for common laboratory conditions with a known accuracy, typically 0.5%. Given the success of the model's formulaic structure, it is likely to apply to even broader ranges of physical conditions and to other gases that relax by spin–rotation interaction.

Keywords: Spin–rotation; Spin–lattice relaxation; Thermal equilibrium polarization; SF_6; CF_4; C_2F_6; C_4F_8

1. Introduction

Inert fluorinated gases, such as sulfurhexafluoride, tetrafluoromethane, hexafluoroethane, and cyclo-octafluorobutane (SF_6, CF_4, C_2F_6, and c-C_4F_8), have single NMR resonances, and rapid spin–lattice relaxation from spin–rotation interaction [1]. Because they have multiple chemically equivalent fluorine atoms per molecule, and one can signal average very rapidly, they are easy gases to image in porous media, including lungs. Knowledge of the T_1s of these gases for typical laboratory conditions and in mixtures with gases commonly found in lungs has substantial practical application. In lung imaging, the mixture ratio of gases in alveoli changes depending on the ratio of ventilation rate and blood perfusion rate (V/Q), and the T_1 depends on the composition of the mixture. Therefore, one could image V/Q by imaging the T_1, or one could calculate how T_1 weighting will affect a spin density image [2].

To study porous materials, inert fluorinated gases can be imbibed into the pore spaces. When the pores are on the order of or smaller than the bulk gas mean free paths, collisions of gas molecules with pore walls play an important role in changing the rotational states of the molecules. Under these conditions, the relaxation could be used to measure pore sizes, provided that one knows the relaxation under bulk conditions for comparison [3,4]. Knowing the bulk gas relaxation is also important for comparison in evaluating the extent to which adsorption on pore surfaces affects relaxation [3,5–7].

Because the relaxation is dominated by spin–rotation interaction mediated by molecular collisions, the bulk gas relaxation rates are, in principle, highly predictable. There have been measurements of coupling constants and collision cross sections [8–27] that clearly lay out

* Corresponding author. Fax: +1 505 244 0018.
E-mail address: dkuethe@nmr.org (D.O. Kuethe).

1090-7807/$ - see front matter © 2005 Elsevier Inc. All rights reserved.
doi:10.1016/j.jmr.2005.07.022

the physical framework, but to calculate a given T_1 often requires determining whether the desired range of physical parameters has been explored, sifting through different parameterizations of relaxation equations, and interpolating between tabulated parameters, after which it can be difficult to calculate the accuracy of the result. We present a unified calculation for common laboratory conditions so that a computer program will generate T_1 within a known accuracy if given pressure, temperature, and mixture composition.

To develop the calculational scheme, we made careful measurements that spanned much of the parameter space of interest and then developed equations with a small number of adjustable parameters capable of fitting the entire data set. We drew from existing physically motivated equations for relaxation, molecular collision frequencies, and equation of state. We then judiciously added parameters when doing so substantially improved the fit to our data. The equations, together with their fitted parameter values, can be used to interpolate between the experimental conditions and, with somewhat less confidence, to extrapolate beyond them.

The basic relation of the relaxation rate to the molecular collision frequency was stated in Bloembergen's doctoral dissertation [28] for hydrogen gas. We begin with the work of Courtney and Armstrong [13], whose physically motivated equations for fluorinated gases came explicitly from [10,23–27]. In [13], the molecular collision dynamics were subsumed into a hard-sphere collision cross section parameter that was endowed with a nonlinear temperature dependence. Some studies have used more realistic molecular potential models for collision dynamics as tools for measuring physical constants and deeper understanding of the physics (e.g. [14], see [1]). We use the Lennard-Jones model to take care of some of the temperature dependence in the hope that the remaining dependence is easy to match with a small number of curve-fitting parameters.

2. Methods

2.1. Equations for fitting T_1

Spin lattice relaxation rate by spin–rotation interaction in a pure gas obeys

$$T_1^{-1} = \frac{8\pi^2 I_0 k_B T}{\hbar^2} \times \left[C_i^2 \frac{\tau_1}{1+(\omega_I-\omega_J)^2\tau_1^2} + \frac{4}{45} C_a^2 \frac{\tau_2}{1+(\omega_I-\omega_J)^2\tau_2^2} \right], \quad (1)$$

where I_0 is the moment of inertia of the molecule, $\hbar$ is Plank's constant, C_i and τ_1, and C_a and τ_2, are isotropic and anisotropic coupling constants and correlation times, respectively, ω_I and ω_J are nuclear and molecular Larmor precession frequencies, respectively, T is absolute temperature, and k_B is Boltzmann's constant ([13], from [10,23–27]).

It is commonly assumed that $\tau_1 = \tau_2 \equiv \tau$ because they both arise from molecular collisions. Then, Eq. (1) simplifies to

$$T_1^{-1} = k_1 T \frac{\tau}{1+k_2^2\omega_I^2\tau^2}, \quad (2)$$

where $k_1 = \frac{8\pi^2 I_0 k_B T}{\hbar^2}\left(C_i^2 + \frac{4}{45}C_a^2\right)$ and $k_2 = 1 - \frac{\omega_J}{\omega_I} \cong 1$ because $\omega_I \gg \omega_J$. To explicitly introduce molecular collision frequency f, we introduce a temperature dependent factor, $b = k_2/\omega_e$, and a coupling constant, $a = k_1/k_2$, where $\omega_e \equiv 1/\tau$ is the frequency of collisions that effect spin–rotation relaxation, to obtain,

$$T_1 = \frac{1}{aT}\left(\frac{f}{b} + \frac{b\omega^2}{f}\right), \quad (3)$$

where we now use ω instead of ω_I for the nuclear Larmor frequency. The factor b is the average number of collisions required to effect one spin–rotation exchange reduced by the minor deviation of k_2 from unity, so it represents a degree of ineffectiveness for molecular collisions to cause a spin–rotation event and $f/b = \omega_e/k_2 \cong \omega_e = 1/\tau$.

Eq. (3) needs to be modified to accommodate the possibility of a relaxation mechanism in the absence of collisions, i.e., to prevent $T_1 \to \infty$ as $f \to 0$. We do this by introducing the term $c\omega\sqrt{T}$, which models a thermally mediated fluctuation whose effect is proportional to field strength, where c is a fitting parameter. Mechanisms for such intramolecular relaxation might be vibration and rotation around bond axes. Thus,

$$T_1 = \frac{1}{aT}\left(\frac{f}{b} + \frac{\omega^2}{\frac{f}{b} + c\omega\sqrt{T}}\right). \quad (4)$$

To calculate collision frequency, we need to know the number density ρ and the molecular velocity v. We calculate a number density by solving the Clausius equation

$$P = \frac{RT}{\tilde{v}-\beta} - \frac{\gamma}{T(\tilde{v}+\alpha)^2}, \quad (5)$$

for the molar volume $\tilde{v}$. R is the universal gas constant, $\alpha = V_c - \frac{RT_c}{4P_c}$, $\beta = \frac{3RT_c}{8P_c} - V_c$, $\gamma = \frac{27R^2T_c^3}{64P_c}$, where P_c and T_c are critical pressure and temperature, and V_c is molar volume at P_c and T_c. Then, we force the number density through its known value at STP by setting

$$\rho = \begin{cases} \rho_h \text{ for } \rho_h \geqslant \rho_{STP}, \\ \rho_l \text{ for } \rho_h < \rho_{STP}, \end{cases} \quad \text{where } \rho_h = \rho_{STP}\rho_{Cl}^* \quad (6)$$
$$\text{and } \rho_l = \rho_h\rho_{Cl}^* + \rho_{Cl}(1-\rho_{Cl}^*),$$

where ρ_{Cl} and ρ_{Cl}^* are the number density and amagat density, respectively, according to the Clausius equation

of state. That is, $\rho^*_{\mathrm{Cl}} = \frac{\rho_{\mathrm{Cl}}}{\rho_{\mathrm{Cl,STP}}}$, where STP ⇒ 273.15 K and 101325 Pa.

We allow for the average molecular velocity to be slightly greater than the Boltzmann velocity at high number densities, due to spending time in one another's attractive potentials, by introducing a curve-fitting parameter q, which is near one:

$$v = \left[1 - q\left(1 - \frac{\rho}{\rho_{ideal}}\right)\right]\sqrt{\frac{8k_{\mathrm{B}}T}{\pi m}}, \tag{7}$$

and where m is molecular mass. The average approach velocity of a species i and the fluorinated gas of interest is

$$\begin{aligned}\bar{v}_i &= \frac{1}{6vv_i}\left[(v^2 + v_i^2 + 2vv_i)^{\frac{3}{2}} - (v^2 + v_i^2 - 2vv_i)^{\frac{3}{2}}\right] \\ &= \frac{1}{3\max(v, v_i)}\left[\min(v, v_i)^2 + 3\max(v, v_i)^2\right],\end{aligned} \tag{8}$$

where v and v_i are the average molecular velocities of the fluorinated gas and species i, respectively. For a pure gas, this simplifies to $\bar{v} = \frac{4v}{3}$.

With density and velocity in hand, the collision frequency with a species i is then

$$f_i = \Omega_i \rho_i \pi \sigma_i^2 \bar{v}_i, \tag{9}$$

where Ω_i is the Lennard-Jones collision integral, interpolated from Appendix Table I–M, column $\Omega^{(1,1)*}$ in [29]. Ω_i is the frequency of collisions between Lennard-Jones molecules divided by the frequency of collisions of hard spheres of the same diameters. Ω_{i} is a function of temperature, specifically of the dimensionless temperature $t^* = \frac{k_{\mathrm{B}}T}{\sqrt{\varepsilon\varepsilon_i}}$, where ε and ε_{i} are the respective Lennard-Jones energy parameters. Ω_i is close to 1, ranging from about 1.5 to 0.95 from low to high temperatures, respectively (Fig. 1A), $\sigma_i = (\sigma + \sigma_{(i)})/2$, where σ and $\sigma_{(i)}$ are the respective Lennard-Jones diameters of the inert fluorinated gas and species i. The particular $\sigma_{(i)}$ and ε_i we chose from [29] appear in Table 1, along with physical parameters.

With the temperature dependence of collision cross section modeled by Lennard-Jones collisions, the remaining temperature dependence for relating spin–rotation interaction to collisions (Fig. 1B) was modeled by setting

$$b = \frac{1}{s\Omega + d}, \tag{10}$$

where s and d are curve-fitting parameters, and Ω is Ω_i for pure fluorinated gas.

For a mixture of gases, we assume

$$\frac{\omega_e}{k_2} = f/b + f_1/b_1 + f_2/b_2 + \cdots + f_n/b_n, \tag{11}$$

where each b_i is approximately the average number of collisions with species i that effect one spin–rotation exchange in the fluorinated gas. We introduce a curve-fitting parameter ζ_i for each species i such that

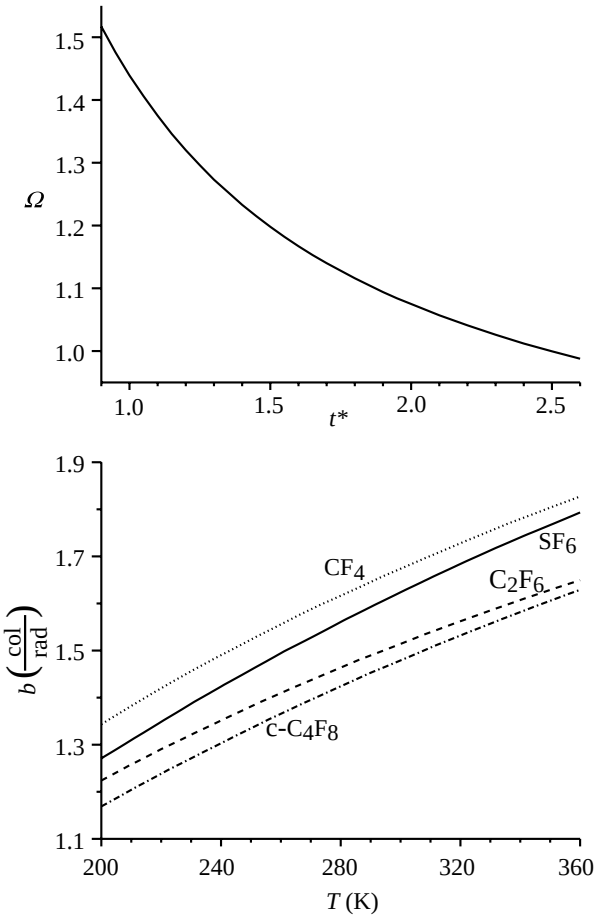

Fig. 1. Temperature dependence of collision cross sections. The top graph shows Ω, the ratio of Lennard-Jones collision frequency to hard sphere collision frequency as a function of the dimensionless temperature, t^*. Lennard-Jones molecules interact less at high temperatures than low compared to hard spheres. The lower graph shows b, the average number of collisions to effect spin–rotation interaction vs. temperature for each gas. Effective changes in rotational state occur even less often at high temperatures compared to low than do changes in translational state.

$$b_i = \zeta_i b\sqrt{\frac{m}{m_i}}. \tag{12}$$

The ζ_i depart from one to the extent that the effect of collisions on rotation departs from scaling with linear momentum transfer. With this formulation, the temperature dependence of the b_i follow that of b.

For the ith component in a mixture, we set

$$q_i = 3.1\left[V_c - N_{\mathrm{A}}\frac{4}{3}\pi\left(\frac{\sigma_i}{2}\right)^3\right], \tag{13}$$

where V_{c} is the critical molar volume in $\mathrm{m^3\,kmol^{-1}}$ or $1\,\mathrm{mol^{-1}}$ and N_{A} is Avogadro's number, unless the mixture species was one of the fluorinated gases for which we had already determined q. The factor 3.1 roughly agrees with the values of q that we determined for SF_6, C_2F_6, and c-C_4F_8. For CF_4, q is not well determined because under our experimental conditions, $\rho/\rho_{\mathrm{ideal}}$ is very close to 1.

Table 1
The particular Lennard-Jones and physical parameters used

Species	σ (Å)	ε/k_B(K)	$\frac{\rho_{\text{ideal}}(\text{STP})}{\rho(\text{STP})}$	P_c (kPa)	T_c(K)	V_c (m^3/kmol)
SF_6	5.3	201	0.98538	3759.00	318.69	0.19805
CF_4	4.68	140	0.99503	3739.00	227.59	0.13993
C_2F_6	5.3	220	0.98741	2980.00	292.85	0.22700
c-C_4F_8	7.03	222.6	0.95675	2786.00	388.45	0.32305
N_2	3.8	60	0.99962	3400.00	126.26	0.090091
O_2	3.48	103	0.99905	5043.00	154.58	0.073405
CO_2	3.96	193	0.99321	7381.50	304.19	0.094052
H_2O	2.641	809.1	0.98020	22120	647.25	0.057600
He	2.551	10.5	1.0004	229.00	5.20	0.057753
Ne	2.8	33	1.0006	2720.00	44.44	0.041738
Ar	3.5	110	0.99900	4864.00	150.72	0.075262
Kr	3.64	180	0.99938	5490.00	209.4	0.092239
Xe	4.2	200	0.99559	5838.00	289.74	0.11880
CH_4	3.809	146	0.99773	4640.00	191.05	0.098713
C_2H_6	4.4	226	0.98962	4914.30	305.5	0.14172
CF_3C1	4.92	222	0.99852	3870.60	302.0	0.18076

For pure gases, we need to determine five parameters: a, s, d, c, and q. For mixtures, we need a ζ_i for each additional species.

To curve fit T_1 data, we minimized the vertical distances of data from curves, $D_{\text{abs}} = \sum_j w_j |T_{1j} - c_j|$, where c_j are the curve-fit values, and w_j are weights that are equal to the reciprocal of the standard deviation of each T_{1J}, $w_j = 1/\text{SD}(T_{1j})$, rather than the least square error $D_{\text{sq}} = \sum_j w_j^2 (T_{1j} - c_j)^2$, which is unduly influenced by outlying data. The normalized fit statistic for D_{abs} is $\text{NFS} \equiv \frac{D_{\text{abs}} - \sqrt{\frac{2}{\pi}} n_f}{\sqrt{n_f}}$, which approaches a normal distribution with mean zero and variance one for degrees of freedom $n_f > 30$. If one knew the $SD(T_{1j})$ with certainty, values less than 2 would indicate that the data support the model within the limits of measurement. Values less than -2 indicate an unexpectedly good fit. We also report the mean percentage deviation (MPD), which is D_{abs} with each term divided by T_{1j} and the w_j adjusted to sum to 1.

$\text{SD}(T_{1j})$ were calculated as $\text{SD}_{CV}(T_{1j}) + E_{T_{1j,P}} + E_{T_{1j,T}}$, where $\text{SD}_{\text{CV}}(T_{1j})$ is the standard deviation of T_1 from the covariance matrix of the inversion-recovery curve fit, and $E_{T_{1j,P}}$ and $E_{T_{1j,T}}$ are the errors in T_1 obtained by varying pressure and temperature within their precision, using the current parameters of the model. Because the w_j affect the fit, the calculation is iterated until there is no change in the fit. For gas mixtures, we also add the error in T_1 that results from the precision with which we prepared the mixture.

2.2. Measuring T_1s

We used a standard inversion recovery sequence with a repetition time of at least 8 T_1 and at least 50 different interpulse delays. When FIDs were off-resonance,they were set to zero frequency by computation. When they were noisy, the portions with a signal-to-noise ratio less than three were discarded. To eliminate truncation artifacts, the FIDs were combined with their mirror images so that the periodic extension would be continuous. After a discrete Fourier transform, the sum of the 20 lowest frequency components of the real part was the datum for a given interpulse delay. The data were fit to a three-parameter exponential recovery curve with a standard least square fitting algorithm.

Our 75.6 MHz data are from the 1.89 T 30 cm bore Oxford magnet with Tecmag Libra console at New Mexico Resonance (N.M.R.). Our 283 MHz data come from the 7 T JEOL system at New Mexico Tech., Department of Chemistry (NMT).

2.3. Measuring pressure, temperature, and mixture composition

For data in which we varied the pressure and temperature of pure gas at N.M.R., we used an Omega PX303-100A5V absolute pressure transducer, calibrated at two pressures: barometric pressure measured with a mercury manometer, and the vacuum of a two-stage vacuum pump. Assuming that the response is linear, we took the error in our pressure measurements to be half the measurement division or ± 50 Pa.

The temperature of the gas sample was measured with a copper-constantan thermocouple glued with epoxy through a hole in the side of the polycarbonate sample container. The Omega HH507 temperature gauge tended to drift by up to 0.3 K. We found no bias with the known temperatures of dry ice in a pure CO_2 atmosphere, of covered boiling distilled water at our local barometric pressure, or of the temperature of ice surfaces in ice water. We took the error in our temperature measurement to be ± 0.15 K.

To obtain low or high temperatures, we passed cold or room temperature N_2 gas over a homemade heater controlled by an on/off switch according to a thermistor reading in a downstream temperature chamber, which consisted of a 41.5 mm ID polycarbonate tube surrounded by a 2 mm layer of Nanopore 0.0036 W/mK thermal insulation that consisted of vacuum-packed carbon impregnated SiO_2 particles [30]. The sample container was located 30 cm downstream from the thermistor and provided enough thermal inertia so that, despite the on/off heater control, the thermocouple in the sample did not show oscillations more than ± 0.15 K.

For the pure gas data collected at 283 MHz using the 7 T JEOL system at NMT, we calibrated the Omega PX303-100A5V absolute pressure transducer at N.M.R. and transported it to NMT to make sure that it agreed with the Baratron pressure transducer on the MKS gauge. We used a homemade 1 m long 5 mm Pyrex N.M.R. tube for a convenient gas-tight connection that reached to the center of the magnet. The commercial JEOL temperature controller was set to 303 K, slightly above room temperature, to provide stable control.

Data for gas mixtures at 75.6 MHz were obtained at N.M.R. at room temperature (measured with a copper-constantan thermocouple taped on the side of a glass sample container, which was wrapped with closed-cell pipe insulation) and pressure (measured with the mercury barometer, and approximately 84 kPa at our altitude). The glass sample container was drawn down at both ends and fitted with two small mylar balloons. The balloons were flaccid to ensure that the pressure inside was barometric.

To produce known mixtures, we introduced known volumes of two gases, measured with two 140 ml plastic syringes that had the same cross sections, volume markings, and slight tapers (as measured with a dial caliper). To make the syringes suitable for delivering pure gases, we held the plunger in a drawn position and exposed them to vacuum for 30 min to remove any sorbed contaminant gases. The error in mixture was calculated from the proportions represented by the finest divisions on the syringes.

2.4. Comparison with data tabulated by number density

Many prior works use samples of known number density, which avoids issues of equation of state when studying relaxation. We incorporate an equation of state because being able to calculate T_1s from pressure and temperature is important for the convenience of a T_1 calculator. As a consistency check, we make sure that our model fits data taken from known number-density samples. Johnson [17] provides an extensive set of such T_1 data for SF_6 and CF_4. His sample containers were filled by condensing known volumes of gases at low pressures (at or below 20 kPa) into known volumes. Thus, his number densities are correct if we assume that low-pressure gases obey the ideal gas equation. Some of the pressures are as high as 15 atm, which gives us an opportunity to test an extrapolation beyond our physical conditions.

To apply our model to Johnson's data, we use the Clausius equation to calculate a pressure from his number density and temperature and then use that pressure to calculate the number density for an ideal gas. We then use the ratio of Johnson's number density to the ideal number density to calculate the average molecular velocity from Eq. (7), using the q factor that we determined from our data. We let the other four parameters (a, s, d, and c) vary to see if the curve fit will yield the same values as ours.

3. Results

3.1. Pure gas data

To collapse many data from different gases and a variety of physical conditions onto a few graphs, we rearrange Eq. (4)

$$\frac{T_1 aT}{\omega} = \frac{f}{b\omega} + \frac{1}{\frac{f}{b\omega} + c\sqrt{T}} \quad \text{or} \quad T_1^* = f^* + \frac{1}{f^* + \omega^*_{\sqrt{T}}}, \tag{14}$$

where $T_1^* = \frac{T_1 aT}{\omega}$ is a dimensionless T_1, $f^* = \frac{f}{b\omega}$ is a dimensionless f, and $\omega^*_{\sqrt{T}} = c\sqrt{T}$ is a dimensionless frequency proportional to $\sqrt{T}$, and note that to the extent that $\omega^*_{\sqrt{T}}$ is small compared to f^*, all data should collapse onto the curve $T_1^* = f^* + 1/f^*$. Indeed, our $\omega^*_{\sqrt{T}}$'s all are less than 0.236 f^*, so when we plot T_1^* *vs.* f^*, we see that $T_1^* = f^* + 1/f^*$, except for small variable departures to lower T_1^* near and to the left of the T_1 minimum.

Fig. 2 shows 376 pure gas data points for the four gases, SF_6, CF_4, C_2F_6, and c-C_4F_8, plotted on such axes along with the curve for the model. The physical conditions are listed on the figure. The parameters for the curve fits appear in Table 2 for each gas. The error bars plotted are $\pm 2\mathrm{SD}(T_{1j})$. The points used to plot the data are larger than most of the error bars. In the inset, the portion around the T_1 minimum is expanded with thinner lines and dots. This is the region where we expect to see the data and model depart below $T_1^* = f^* + 1/f^*$ to a small degree, depending on gas species and temperature. The exceptional species is c-C_4F_8, for which c, the fitting parameter defined in Eq. (4), is essentially zero. This may stem from the fact that c-C_4F_8 is a tightly constrained molecule.

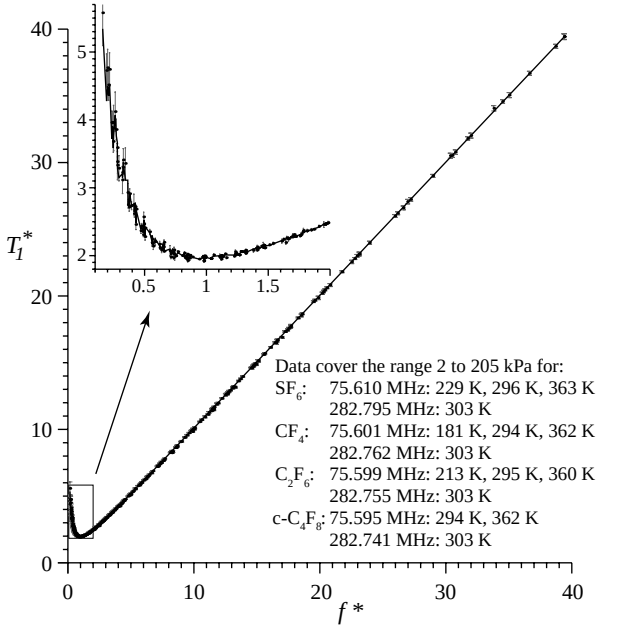

Fig. 2. T_1 data from SF_6, CF_4, C_2F_6, and c-C_4F_8 plotted on axes of dimensionless T_1 vs. dimensionless collision frequency. The data (dots) are a good fit to the model (line). Both trace the curve $T_1^* = f^* + 1/f^*$, except for expected departures near and to the left of the T_1 minimum (expanded in inset). The line consists of straight segments connecting the model's predicted T_1 for the conditions and species of each datum, so it follows a jagged path near and to the left of the T_1 minimum.

Table 2
The five curve-fitting parameters for the pure gas T_1 data

Species	a (rad s^{-2} K^{-1})	s (rad col^{-1})	d (rad col^{-1})	c (K$^{-1/2}$)	q	NFS	MPD (%)
SF_6	8.043e+09 ± 2.514e+07	0.7067 ± 7.455e−3	−0.2325 ± 7.974e−3	3.032e−3 ± 1.929e−4	0.4978 ± 0.05329	4.570	0.4550
SF_6 using virial ES	8.041e+09 ± 2.621e+07	0.7277 ± 4.871e−3	−0.2595 ± 5.493e−3	3.059e−3 ± 2.003e−4	Fixed at 0.4978	4.307	0.4244
CF_4	6.738e+09 ± 1.899e+07	0.8516 ± 7.411e−3	−0.2969 ± 7.221e−3	1.865e−3 ± 1.673e−4	0.08738 ± 0.07374	5.650	0.4725
C_2F_6	2.027e+09 ± 6.699e+06	0.5976 ± 6.790e−3	−0.08502 ± 7.783e−3	8.881e−4 ± 1.996e−4	0.569 ± 0.0423	7.866	0.7884
c-C_4F_8	5.125e+08 ± 1.734e+06	0.6784 ± 8.814e−3	−0.1745 ± 9.566e−3	−1.211e−09 ± 2.361e−4	0.6543 ± 0.02547	0.3586	0.3521

±1 SD from covariance matrix.
MPD, weighted mean percentage deviation of T_1 from curve.
NFS, normalized fit statistic has a normal distribution with variance 1 and expectation of zero if the model fits the data within the error bars shown in Fig. 2.

The mean percentage deviation values in Table 2 indicate precise agreement between our model and the data. Nonetheless, with the exception of the c-C_4F_8 data, which have a NFS = 0.359, the other NFS range from 4.31 to 7.37 indicating that the model does not fit the data within the limits of measurement. Because these statistics suggest a systematic error, it is important to examine the possibility of biases in measurement that could escape our precision of calibration. We could have missed a 0.1 K bias in the temperatures of both dry ice and boiling water. Our mercury manometer could be miscalibrated by 0.3 mm, an error of 0.05% in measuring length, which would translate to a bias of 270 Pa at our highest pressure readings. If we allow ±0.25 K and ±320 Pa rather than ±0.15 K and ±50 Pa for errors in measurement of temperature and pressure, respectively, to accommodate these conceivable biases, then the NFS for our poorest fitting data set, the C_2F_6 data, becomes −1.40, rather than 7.87. This negative NFS value indicates a fit that is somewhat better than expected. Thus, we cannot rule out undetectable bias as an explanation for the high normalized fit statistics, so we conclude that we have done as well as we could with our equipment.

A simple procedure to reverse the curve-fitting process and obtain bounds on the model's prediction of T_1s is to vary the temperature at which one seeks the T_1 by ±0.25 K and the pressure by ±320 Pa and take the lowest and highest of the four resulting values. This procedure results in remarkably narrow ranges of about 0.5 to 1% for common laboratory conditions.

3.2. Comparison of previous data with known number density

Johnson's [17] pure gas data, tabulated by number density, allow us to check how well we dealt with the equation of state. Fig. 3 shows Johnson's 279 data points for pure SF_6 and CF_4 on the same axes as Fig. 2. The curve-fitting parameters appear in Table 3. The highest pressures we calculated for the given number densities for SF_6 and CF_4 were approximately 14 and 15 atm, respectively, so these data test an extrapolation beyond our pressure range, which extends to only 2 atm. There are no individual Larmor frequencies given with Johnson's data. However, given that a and ab should not vary with Larmor frequency, we found the frequencies (184.7 and 184.5 MHz, for SF_6 and CF_4, respectively) for which his data produce a value for the parameter a that matches ours, and they are consistent with the nominal hydrogen frequency of his magnet (Nicolet 200 MHz, 4.7 T). We assumed that his number

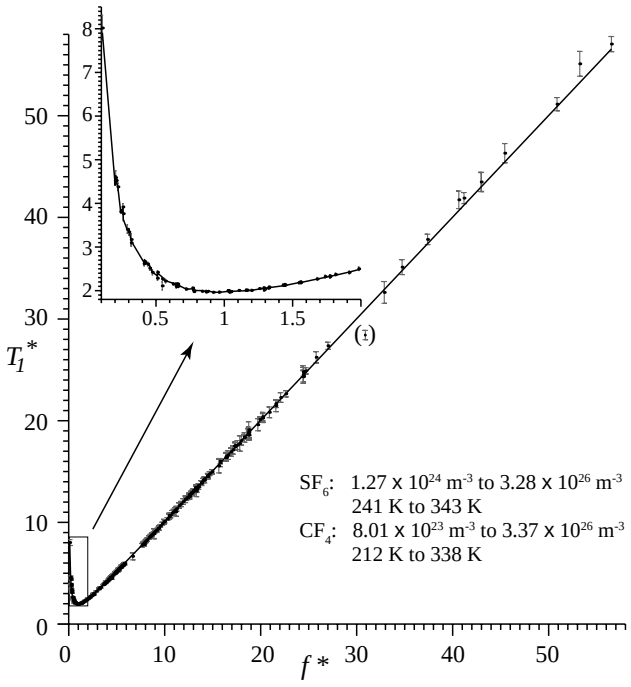

Fig. 3. T_1 data for known number densities of pure SF_6 and CF_4 from Johnson's thesis [17] plotted on the same axes as Fig. 2. The agreement of model and data indicates that we made a good choice for equation of state and that our model extrapolates well to pressures of 14 atm. The curve-fitting parameters are in Table 2. The larger error bars on the right reflect how the samples are prepared with known number densities ±1% as opposed to monitoring the pressure. The datum in parentheses was excluded from the curve fit.

Table 3
Four curve-fitting parameters for Johnson's pure gas data

Species	a (rad s^{-2} K^{-1})	s (rad col^{-1})	d (rad col^{-1})	c (K$^{-1/2}$)	NFS	MPD (%)
SF_6	8.043e+09 ± 3.295e+07	0.7386 ± 8.338e−3	−0.2696 ± 9.43e−3	2.105e−3 ± 1.895e−4	−0.2489	0.5397
CF_4	6.738e+09 ± 2.965e+07	0.9526 ± 1.365e−2	−0.4042 ± 1.422e−2	1.205e−3 ± 1.616e−4	0.4645	0.6703

NFS relative to error bars are shown in Fig. 3.

densities and temperatures were correct to within 1% and ±0.15 K, respectively. The resulting error bars and fit statistics appear appropriate. Our model works well with Johnson's data, and the common parameters agree.

As a second comparison, we tried fitting our SF_6 data with the virial equation of state [31] that [13] used instead of the Clausius equation. The results (Table 2) are the same.

3.3. Gas mixtures

Fig. 4 shows that our model for T_1s of mixtures fits the data using the ζ_i in Table 4. The dimensionless f^* for these mixtures is $(f/b + f_1/b_1)/\omega$. To obtain bounds for predicted T_1s of mixtures, one can follow the procedure of bracketing the temperature and pressure within ±0.25 K and ±320 Pa, as suggested above, while bracketing ζ_i with ± its standard deviation.

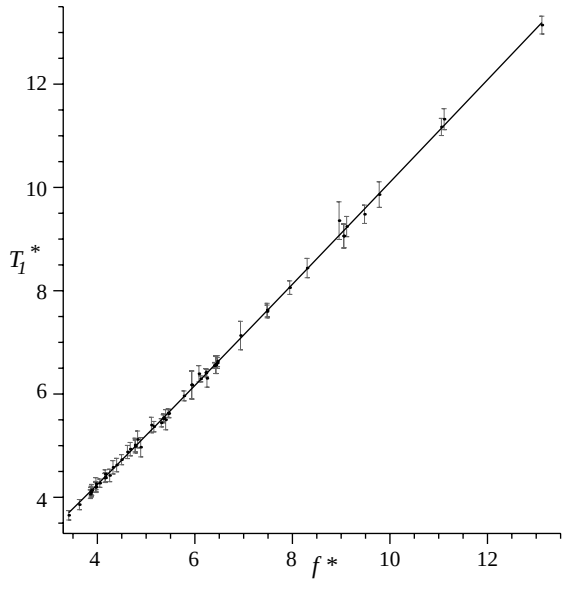

Fig. 4. T_1 data for mixtures of SF_6, CF_4, C_2F_6, or c-C_4F_8 with other gases, as listed in Table 4, plotted on dimensionless axes. The model fits the data.

Johnson's thesis provides a wealth of data for gas mixtures that our model can readily accommodate, so we analyzed the gas mixtures for which we had Lennard-Jones parameters to provide a large variety of ζ_i parameters. Fig. 5 shows Johnson's data for the mixtures represented by entries in Table 5. The outliers in the center of the graph are the Ne data, which show sufficient scatter to conclude that the unusually low ζ_i is probably wrong. The few outliers to the left are He data and, while scattered, the ζ_i appear reasonably well determined. The remaining data behave extremely well.

The ζ_i parameters appear to vary slightly with temperature, indicating that the b_i may not track the temperature dependence of b. This is reminiscent of Jameson and Jameson's [19] finding that there are variations in the exponents of temperature that determine the collision cross section, depending on CF_4's collision partner. However, the pattern according to partner (CH_4, C_2H_6, Ar, Kr, Xe, CO_2, or SF_6) in [19] appears uncorrelated to that in Table 5, even after taking into account the effect that different $\frac{\sqrt{\varepsilon\varepsilon_i}}{k_B}$ for Lennard-Jones molecules would have on the exponents for hard spheres. In both cases, the temperature effects appear statistically significant and we are at a loss to explain the small discrepancy. However, the tabulated temperature effect is so small (around 8×10^{-4} K^{-1} or less) that for the purposes of calculating T_1s for gas mixtures in lungs, it appears safe to measure ζ_i at room temperature.

A stronger trend in the ζ_i is that those molecules that have high moments of inertia for their mass have lower ζ_i. It appears that they are more effective at changing the rotational state of the inert fluorinated gas molecules in collisions.

It would be difficult for us to measure ζ_i for water vapor. However, the SF_6 T_1s calculated for gas compositions in lungs, assuming normal V/Q, agree with those we measure in healthy rats [2] when we set ζ_i for H_2O to 1.1.

Table 4
ζ parameters for gas listed on top in gas listed at side at room temperature

	SF_6	CF_4	C_2F_6	c-C_4F_8
CF_4				0.9738 ± .00489
c-C_4F_8		1.291 ± .00785		
N_2	1.295 ± .00902	1.134 ± .00539	1.235 ± .0162	1.275 ± .0152
O_2	1.215 ± .00612	1.063 ± .00402	1.178 ± .00701	1.335 ± .0146
CO_2	1.015 ± .00518	0.8813 ± .00147	0.9719 ± .00357	0.962 ± .00424

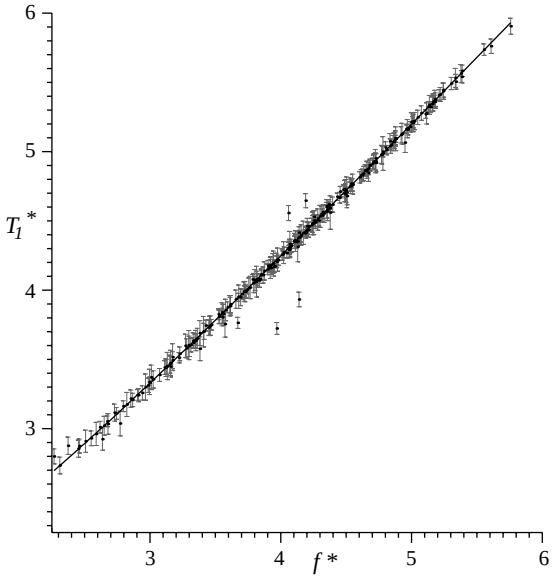

Fig. 5. Johnson's T_1 data for mixtures of SF_6 or CF_4 with other gases, as listed in Table 5. The curve uses the ζ_i in Table 5 and our *a*, *s*, *d*, *c*, and *q* parameters in Table 2. With the exception of the neon mixtures that account for the outliers near the center, the model fits the data well.

At higher pressures than we investigated here, the spin–rotation relaxation rates could become sufficiently low that dipole interactions with paramagnetic O_2 may become significant [20,22]. This raises the question of whether we can safely ignore them. Given our simplified analysis, this additional relaxation would express itself as larger ζ_i with odd temperature and field dependence. The ζ_i for CF_4–O_2 at 184.1 MHz in Table 5 (1.086 ± 0.00448) is close to, but significantly higher than the one at 75.59 MHz in Table 4 ($1.063 \pm .00402$). However, it does not appear to be unusually high compared to other collision partners with similar mass distribution. Among our data, the relaxation rate for c-C_4F_8 is the slowest of the fluorinated gases, so this is where we would most expect to see an artificially high ζ_i due to O_2's paramagnetism. The value of ζ_i for c-C_4F_8–O_2 ($1.335 \pm .0146$) is similar to that for c-C_4F_8–N_2 ($1.275 \pm .0152$), while it is less than that for N_2 for the other three gases, SF_6, CF_4, and C_2F_6 (e.g., SF_6–O_2 $1.215 \pm .00612$ vs. SF_6–N_2 $1.295 \pm .00902$). Thus, it appears that we may be close to the regime for which one would want to take the paramagnetism of O_2 into account. For pressures above 1 atm or Larmor frequencies above 75.6 MHz, our calculations for O_2 mixtures should not be extrapolated without experimental verification.

4. Conclusions

Eqs. (4)–(13) and curve fitting parameters in Tables 2, 4, and 5 allow one to calculate T_1s of SF_6, CF_4, C_2F_6, and c-C_4F_8 for common laboratory conditions. They should be especially useful for spatially resolved V/Q measurements in pulmonology. The particular physical parameters we used appear in Table 1. The accuracy is 0.5 to 1% and is explicitly calculated by varying temperature and pressure by ± 0.25 K and ± 320 Pa, respectively, and taking the lowest and highest results. For gas mixtures, T and P are varied using ζ_i plus its standard deviation and varied using ζ_i minus its standard deviation.

Table 5
ζ parameters for SF_6 and CF_4 mixtures in Johnson's Thesis

	SF_6		CF_4	
	T (K)	ζ	T (K)	ζ
He	293.0	1.204 ± 0.0602	293.0	1.098 ± 0.0218
He	332.4	1.192 ± 0.0648	322.3	1.134 ± 0.0210
CH_4	252.7	1.527 ± 0.0117	252.7	1.209 ± 0.00711
CH_4	267.7	1.538 ± 0.0125	267.4	1.213 ± 0.00465
CH_4	293.0	1.562 ± 0.0109	293.0	1.235 ± 0.00437
CH_4	322.8	1.605 ± 0.0102	322.4	1.263 ± 0.00754
Ne	293.0	0.5107 ± 0.0193	293.0	0.5794 ± 0.00926
C_2H_6	252.7	1.199 ± 0.00461	252.7	1.029 ± 0.00382
C_2H_6	267.7	1.211 ± 0.00491	267.8	1.033 ± 0.00327
C_2H_6	293.0	1.232 ± 0.00398	293.0	1.050 ± 0.00168
C_2H_6	322.8	1.269 ± 0.00509	322.4	1.075 ± 0.00288
Ar	252.5	1.229 ± 0.0101	253.0	1.072 ± 0.00351
Ar	267.7	1.238 ± 0.0188	267.4	1.077 ± 0.00389
Ar	293.0	1.214 ± 0.00687	293.0	1.077 ± 0.00252
Ar	322.4	1.240 ± 0.0126	322.3	1.091 ± 0.00645
CO_2	252.7	1.014 ± 0.00348	252.7	0.8726 ± 0.00237
CO_2	267.7	1.020 ± 0.00265	267.8	0.8724 ± 0.00216
CO_2	293.0	1.033 ± 0.00270	293.0	0.8803 ± 0.00162
CO_2	322.8	1.058 ± 0.00346	322.4	0.9055 ± 0.00223
Kr	252.5	1.195 ± 0.00578	253.0	1.151 ± 0.00556
Kr	267.7	1.192 ± 0.00440	267.4	1.153 ± 0.00391
Kr	293.0	1.192 ± 0.00243	293.0	1.162 ± 0.00296
Kr	322.8	1.212 ± 0.00522	322.3	1.198 ± 0.00764
CF_4/SF_6	252.5	0.9962 ± 0.00356	252.5	1.076 ± 0.00306
CF_4/SF_6	267.8	0.9989 ± 0.00277	267.8	1.076 ± 0.00282
CF_4/SF_6	293.0	1.004 ± 0.00193	293.0	1.083 ± 0.00170
CF_4/SF_6	322.3	1.024 ± 0.00232	322.3	1.091 ± 0.00218
CF_3Cl	252.7	0.9912 ± 0.00228	252.7	1.017 ± 0.00267
CF_3Cl	267.7	0.9939 ± 0.00192	267.8	1.022 ± 0.00205
CF_3Cl	293.0	0.9969 ± 0.00263	293.0	1.022 ± 0.00171
CF_3Cl	322.8	1.014 ± 0.00212	322.7	1.031 ± 0.00212
Xe	252.5	1.299 ± 0.00516	253.0	1.324 ± 0.00589
Xe	267.7	1.301 ± 0.00324	267.4	1.331 ± 0.00410
Xe	293.0	1.303 ± 0.00235	293.0	1.346 ± 0.00191
Xe	332.4	1.328 ± 0.00766	322.7	1.360 ± 0.00467
O_2			293.0	1.086 ± 0.00448

Acknowledgments

We thank Cathy F.M. Clewett and Natalie L. Adolphi for technical assistance, Andrew F. McDowell for suggestions on the manuscript, Eiichi Fukushima and Larry Werbelow for helpful discussions, Doug Smith for the Nanopore insulation, and NIH Grants R29HL57967 and R01EB002072 for financial support.

References

[1] R.L. Armstrong, Nuclear magnetic relaxation effects in polyatomic gases, Magn. Reson. Rev. 12 (1987) 91–135.

[2] D.O. Kuethe, A. Caprihan, H.M. Gach, I.J. Lowe, E. Fukushima, Imaging obstructed ventilation with NMR using inert fluorinated gases, J. Appl. Physiol. 88 (2000) 2279–2286.

[3] M.J. Lizak, M.S. Conradi, C.G. Fry, NMR imaging of gas imbibed into porous ceramic, J. Magn. Reson. 95 (1991) 548–557.

[4] A. Caprihan, C.F.M. Clewett, D.O. Kuethe, E. Fukushima, S.J. Glass, Characterization of partially sintered ceramic powder compacts using fluorinated gas NMR imaging, Magn. Reson. Imag. 19 (2001) 311–317.

[5] S.D. Beyea, A. Caprihan, C.F.M. Clewett, S.J. Glass, Spatially resolved adsorption isotherms of thermally polarized perfluorinated gases in Y-TZP ceramic materials using NMR imaging, Appl. Magn. Res. 22 (2002) 175–186.

[6] S.D. Beyea, S.J. Glass, A.A. DiGiovanni, A. Caprihan, Non-destructive characterization of nanopore microstructure: space resolved BET isotherms using NMRI, J. Appl. Phys. 941 (2003) 935–994.

[7] S.D. Beyea, S.L. Codd, D.O. Kuethe, E. Fukushima, Studies of porous media by thermally polarized gas NMR: current status, Magn. Reson. Imag. 21 (2003) 201–205.

[8] R. Blinc, G. Lahajnar, Nuclear-magnetic-resonance relaxation by spin–rotational interactions in the solid, Phys. Rev. Lett. 19 (1967) 685–687.

[9] R.L. Armstrong, E. Tward, Spin–lattice relaxation in dilute gases. II. ^{19}F relaxation in CF_4 and SiF_4, J. Chem. Phys. 48 (1968) 332–334.

[10] R.Y. Dong, M. Bloom, Determination of spin–rotation interaction constants in fluorinated methane molecules by means of nuclear spin relaxation measurements, Can. J. Phys. 48 (1970) 793–804.

[11] S. Mohanty, H.J. Bernstein, Fluorine relaxation by NMR absorption in gaseous CF_4, SiF_4, and SF_6, J. Chem. Phys. 53 (1970) 461–462.

[12] O.P. Revokatov, S.V. Parfenov, Spin-lattice relaxation time in SF_6 in the critical temperature region, JETP Lett. 15 (1972) 103–105.

[13] J.A. Courtney, R.L. Armstrong, A nuclear spin relaxation study of the spin–rotation interaction in spherical top molecules, Can. J. Phys. 50 (1972) 1252–1261.

[14] S. Rajan, K. Lalita, S.V. Babu, Intermolecular potentials from NMR data: II. CH_4, CF_4, and SiF_4, Can. J. Phys. 53 (1975) 1631–1634.

[15] R.J. Finney, M. Wolfe, J. Jonas, NMR study of angular momentum relaxation in fluids. I. compressed CF_4, J. Chem. Phys. 67 (1977) 4004–4011.

[16] M. Wolfe, E. Arndt, J. Jonas, NMR study of angular momentum relaxation in fluids II: mixtures of CF_4 with inert gases, J. Chem. Phys. 67 (1977) 4012–4018.

[17] M.D. Johnson, Gas phase longitudinal nuclear spin relaxation measurements of angular momentum relaxation in SF_6 and CF_4, Ph.D. dissertation, University of California, Davis, 1986.

[18] C.J. Jameson, A.K. Jameson, Effective collision cross-section for SF_6 from nuclear magnetic relaxation, J. Chem. Phys. 88 (1988) 7448–7452.

[19] C.J. Jameson, A.K. Jameson, Relaxation cross sections for the rotational angular momentum vector in CF_4, J. Chem. Phys. 890 (1988) 866–887.

[20] C.J. Jameson, A.K. Jameson, J.K. Kwang, D. Dabkowski, Competition of intra- and intermolecular spin relaxation mechanisms for SF_6 in oxygen gas, J. Chem. Phys. 92 (1988) 5937–5941.

[21] C.J. Jameson, A.K. Jameson, Angular momentum relaxation in binary collisions, comparison of cross sections, J. Chem. Phys. 93 (1990) 3237–3244.

[22] C.J. Jameson, A.K. Jameson, J.K. Kwang, ^{19}F nuclear spin relaxation by intermolecular magnetic dipole coupling. CF_4 and SiF_4 in oxygen gas, J. Chem. Phys. 94 (1991) 172–178.

[23] C.H. Anderson, N.F. Ramsey, Magnetic resonance molecular-beam spectra of methane, Phys. Rev. 149 (1966) 14–24.

[24] P.N. Yi, I. Ozier, C.H. Anderson, Theory of nuclear hyperfine interactions in spherical top molecules, Phys. Rev. 165 (1968) 92–109.

[25] M. Bloom, F. Bridges, W.N. Hardy, Nuclear spin relaxation in gaseous methane and its deuterated modifications, Can. J. Phys. 45 (1967) 3533–3553.

[26] F.R. McCourt, S. Hess, Nuclear magnetic relaxation in a gas of regular molecules, Z. Naturforsch. 25a (1970) 1169–1177.

[27] F.R. McCourt, S. Hess, On nuclear magnetic relaxation in dilute gases of symmetric and spherical top molecules, Z. Naturforsch. 26a (1971) 1234–1236.

[28] N. Bloembergen, Nuclear magnetic relaxation, Ph.D. thesis, University of Leiden (1948), Eq. (4.33), reprinted in: N. Bloembergen (Ed.), Nuclear Magnetic Relaxation: A Reprint Volume, W.A. Benjamin, New York, 1961.

[29] J.O. Hirschfelder, C.F. Curtiss, R.B. Bird, Molecular Theory of Gases and Liquids, Wiley, New York, 1954.

[30] D.M. Smith, W.C. Ackerman, A. Maskara, Compositions and insulation bodies having low thermal conductivity, U.S. Patent #5,877,100.

[31] K.E. MacCormack, W.G. Schneider, Intermolecular potentials. I. carbon tetrafluoride and sulfur hexafluoride. II. carbon dioxide, J. Chem. Phys. 19 (1951) 849–855.